IOPscience iopscience.iop.org

Home Search Collections Journals About Contact us My IOPscience

A plasmonic terahertz detector with a monolithic hot electron bolometer

This article has been downloaded from IOPscience. Please scroll down to see the full text article.

2009 J. Phys.: Condens. Matter 21 195803

(http://iopscience.iop.org/0953-8984/21/19/195803)

View the table of contents for this issue, or go to the journal homepage for more

Download details:
IP Address: 129.252.86.83
The article was downloaded on 29/05/2010 at 19:35

Please note that terms and conditions apply.

J. Phys.: Condens. Matter **21** (2009) 195803 (6pp) doi:10.1088/0953-8984/21/19/195803

A plasmonic terahertz detector with a monolithic hot electron bolometer

G C Dyer[1], J D Crossno[1], G R Aizin[2], E A Shaner[3], M C Wanke[3], J L Reno[3] and S J Allen[1]

[1] Physics Department, University of California-Santa Barbara, Santa Barbara, CA 93106, USA
[2] Department of Physical Sciences, Kingsborough College, CUNY, Brooklyn, New York 11235, USA
[3] Sandia National Laboratories, Albuquerque, NM 87185, USA

Received 27 April 2008, in final form 6 August 2008
Published 16 April 2009
Online at stacks.iop.org/JPhysCM/21/195803

Abstract
A plasmonic terahertz detector that integrates a voltage-controlled planar barrier into a grating gated GaAs/AlGaAs high electron mobility transistor has been fabricated and experimentally characterized. The plasmonic response at fixed grating gate voltage has a full width at half-maximum of 40 GHz at ∼405 GHz. Substantially increased responsivity is achieved by introducing an independently biased narrow gate that produces a lateral potential barrier electrically in series with the resonant grating gated region. DC electrical characterization in conjunction with bias-dependent terahertz responsivity and time constant measurements indicate that a hot electron bolometric effect is the dominant response mechanism at 20 K.

1. Introduction

Plasmonic detectors offer the possibility of electrically tunable terahertz (THz) detectors for chip-based THz spectroscopy [1–6]. These planar devices are fabricated from wafers using processing very similar to other III–V semiconductor devices and may lend themselves to spectroscopic THz imaging with focal plane arrays. The electrically tuned narrow band response is unique to the 2D plasmonic detector [7, 8], but its application to a detector array requires integrating the relatively narrow band response with a sensitive detection element. In this paper, we will discuss the successful integration of an independently voltage-controlled lateral barrier with a grating gated high electron mobility transistor (HEMT). This scheme retains narrow band tunable THz detection via collective plasmonic excitations of a two-dimensional electron gas (2DEG) while integrating a bolometric element, and substantially improves the sensitivity of the device with respect to earlier generations of grating gated THz detectors [3–5]. This monolithic grating gated HEMT integrates photonics, electronics and plasmonics in a tunable THz detector.

2. THz grating gated HEMT

The intrinsic THz photoresponse of grating gated GaAs/AlGaAs HEMTs is abundantly documented in the literature [3–6, 9, 10]. These studies have shown that a single quantum well (SQW) HEMT with a periodic grating gate couples THz radiation to the 2D plasma oscillations of the 2DEG.

The coupling arises from two mechanisms. First, the grating gate behaves as a polarizer by strongly reflecting radiation polarized along the grating slats and largely transmitting radiation in the perpendicular polarization. For the latter polarization, the spatially modulated terahertz near-field excites the 2D plasmons. Second, the grating gate will produce a periodic spatial modulation of the electron density in the channel and serves to couple the spatially uniform terahertz field to 2D plasmons. Both mechanisms serve to excite 2D plasmons at frequencies [11]

$$f_j \simeq \frac{1}{2\pi}\sqrt{\frac{e^2\overline{n_{2D}}k_j}{2\varepsilon_{\rm eff}\varepsilon_0 m^*}} \quad (1)$$

where e is the electron charge, $\overline{n_{2D}}$ is the effective 2D electron density, $\varepsilon_{\rm eff}$ is an effective permittivity and m^* is the electron effective mass. The k_j are wavevectors defined by the grating gate period l:

$$k_j = \frac{2\pi}{l}j. \quad (2)$$

Thus, the grating gate period l defines the wavevector of a resonant plasmon mode; $j = 1$ corresponds to the fundamental mode and integer values of $j > 1$ correspond to higher harmonics. The effective permittivity $\varepsilon_{\rm eff}$ accounts for the dielectric properties of the layered semiconductor structure and metalization.

 © 2009 IOP Publishing Ltd Printed in the UK

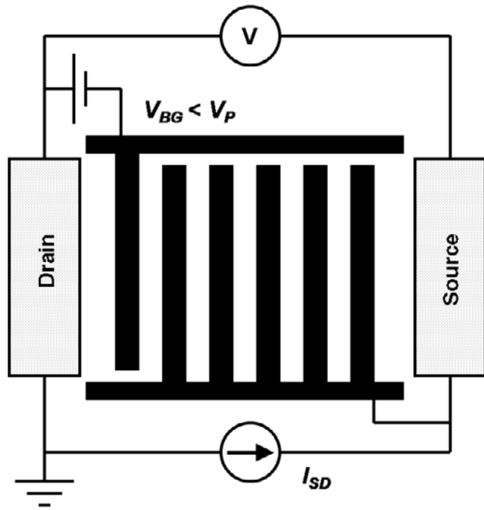

Figure 1. THz grating gated HEMT schematic. The barrier gate is biased with respect to the drain, which is held at ground. The grating gate is shorted to the source contact to ensure that the gate and 2DEG are at the same potential.

By the design of the semiconductor heterostructure, the modulation doping and the grating gate geometry, the resonant frequencies and coupling to the radiation field can be engineered and tuned to provide an essential building block of a THz spectroscopic detector [5]. Resonant absorption of THz radiation at the 2DEG plasma frequency in an SQW HEMT with a grating gate directly produces a change in DC channel conductance. Theoretical models have shown that this can be understood through enhanced electron drag [12] and electrostriction [13]. The latter is particularly important when the 2DEG density has a strong spatial modulation due to the grating gate. This intrinsic THz photoconductive response is fast [14] but lacks sufficient responsivity for direct detection.

The next generation of grating gated detectors integrates an independently biased barrier gate or finger gate [9] to enhance the sensitivity (figure 1). A 50-fold increase in responsivity has been reported by Shaner *et al* [10] when the plasmonic detector is fabricated on a thin membrane and the channel under the barrier or finger gate is biased beyond threshold. Under these conditions, the fully depleted section of the channel appears to act as a bolometric element that senses the change in electron temperature caused by resonant plasmon absorption of the THz radiation. The membrane serves to thermally isolate the bolometric element, thereby enhancing the bolometric response.

With sufficient source drain bias the current–voltage characteristics are extremely nonlinear and exhibit 'short channel' effects analogous to those seen in sub-micron GaAs MESFETs, although the section of the channel under the gate is not sub-micron [15]. Large source drain voltages can cause current to flow due to barrier lowering even though the channel is pinched off. In particular, the strongly pinched-off channel under negative source–drain bias exhibits a very nonlinear 'Schottky-like' characteristic, suggesting that, under appropriate operating conditions, THz rectification could play a significant role in the detector's response. However, here we will discuss only the bolometric behavior of these detectors which appears to dominate the response at cryogenic temperatures.

3. Detector structure

These devices are fabricated from a GaAs/AlGaAs heterostructure (Sandia wafer EA741) having a 30 nm GaAs SQW approximately 200 nm below the surface. The substrate thickness is $\sim$500 μm. Both adjacent AlGaAs layers are Si δ-doped, yielding an electron density in the SQW of 2.1–2.2 $\times 10^{11}$ cm^{-2} and a mobility of at least 10^6 cm^2 V^{-1} s^{-1} at liquid helium temperatures. 1 mm $\times$ 1 mm square isolation mesas are etched through the 2DEG and standard annealed ohmic contacts are fabricated at the source and drain with the grating and contacts covering essentially the entire surface of the mesa. The grating gate metalization between the source and drain consists of Ti/Au slats 2 μm wide spaced by 2 μm for a period $l = 4$ μm. The barrier gate is identical to one of the slats of the grating gate but can be biased independently, allowing the channel to be pinched off, presenting a barrier to current flow (figure 1). The detector is mounted upon a 16-pronged chip carrier with gate, source and drain contacts are wire bonded to adjacent prongs and it is oriented such that incident radiation is polarized orthogonal to the fingers of the interdigitated gate.

4. Device *I*–*V* characteristics

There are a variety of different schemes to electrically bias this detector. Here we discuss the behavior in the configuration illustrated in figure 1. The drain is at ground potential. The barrier gate is negatively biased with respect to the ground. The grating gate is held at the same potential as the source. With a barrier gate voltage beyond pinch off, $V_{\mathrm{BG}} < V_{\mathrm{P}}$, the device becomes highly resistive and the source–drain voltage is dropped across the narrow voltage-induced barrier. The detector source–drain current voltage characteristic becomes very nonlinear under these conditions [9]. However, it is important to realize that in this configuration the electron density under the grating gate does not change when a source–drain bias is applied.

Figure 2 illustrates characteristic current–voltage traces measured at 20 K in a closed cycle refrigerator capable of operation from 10 to 300 K. The barrier gate bias is changed in increments of -100 mV from -650 to -950 mV. Pinch off, V_{P}, occurs between -500 and -600 mV barrier gate bias. At 20 K the mobility of the 2DEG is sufficiently high that it presents little series resistance and the *I*–*V* characteristic is determined solely by the pinched-off region; the *I*–*V* characteristics reflect transport over the gate-controlled barrier. At $V_{\mathrm{SD}} > 0$, the *I*–*V* curve has strong temperature dependence and is exploited in the work described by Shaner *et al* [9, 10].

For $V_{\mathrm{SD}} < 0$, the device shows striking 'Schottky-like' *I*–*V* characteristics with $V_{\mathrm{BG}} < V_{\mathrm{P}}$. This 'short-channel' feature created by the pinched-off barrier is very much like that proposed and discussed by Ryzhii *et al* [16]. Our

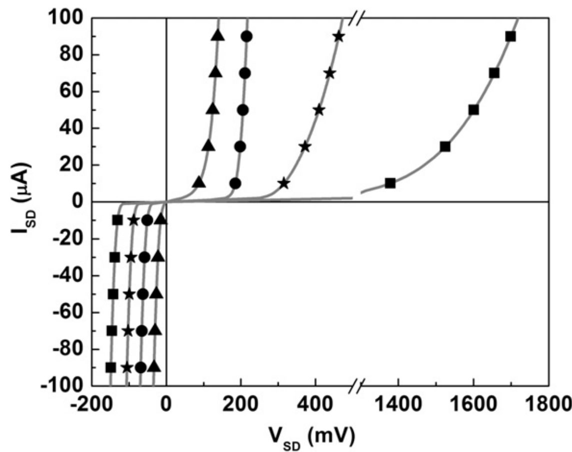

Figure 2. Device I–V characteristics measured at barrier gate biases $V_{BG} = -650$ mV (triangles), $V_{BG} = -750$ mV (circles), $V_{BG} = -850$ mV (stars) and $V_{BG} = -950$ mV (squares), $T = 20$ K.

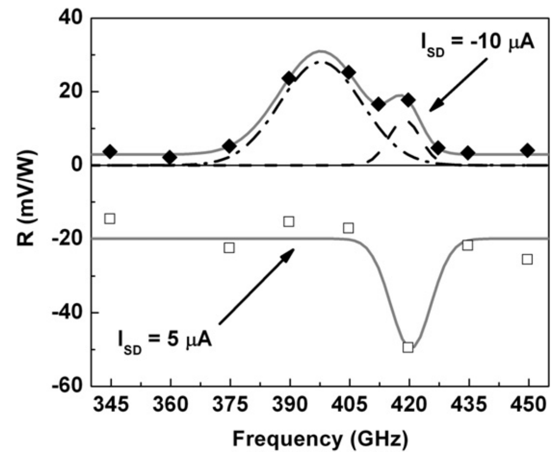

Figure 3. Frequency dependence of detector response at $T = 20$ K for barrier gate bias $V_{BG} = -850$ mV with $I_{SD} = -10\ \mu$A (diamonds) and $I_{SD} = 5\ \mu$A (squares). The solid gray and dashed black traces are included to highlight the resonant features.

voltage-controlled barriers are also similar to the lateral p–n–p junctions fabricated by focused laser-induced diffusion described by Baumgartner *et al* [17]. When a negative source–drain bias is applied, the chemical potential on the source side of the device rises with respect to the barrier and thermally activated electrons produce a rapidly increasing net current. Alternatively, one may consider that the source side of the barrier is lowered and the channel at the source end approaches threshold linearly with respect to source–drain bias. This is consistent with 'short-channel' barrier lowering and it is important to note that the barrier drops at a lesser rate than that at which the source–drain voltage grows [15]. An analogy to a forward-biased Schottky junction on an n-type degenerate semiconductor at low temperature is also suitable, though this picture must be modified because the chemical potential shifts a fraction of a volt for every volt applied between (source and drain) terminals. The barrier gate bias unambiguously controls the barrier height E_B and the latter increases monotonically as the barrier gate is swept beyond pinch off; a more negative source–drain bias is required to turn the current on.

The positive source–drain bias regime, $V_{SD} > 0$, can also be understood in terms of 'short-channel' barrier lowering in a field effect transistor. However, barrier lowering appears to no longer simply scale linearly with source–drain bias in this regime [15]. Under these bias conditions, the barrier height is a more complicated function of both barrier gate bias and source–drain bias due to the proximity of the negatively biased barrier gate and the positively biased grating gate.

The I–V characteristic displayed in figure 2 suggests that the barrier region could respond to absorbed terahertz radiation by direct rectification or by electron heating. The latter mechanism could proceed by heating the entire detector, lattice and electron gas, or the electron gas alone as a hot electron bolometer. Previous work in which thermal isolation was introduced by supporting the grating gated region and barrier region on a thin membrane strongly suggests that the substrate as well as the electron gas is heated. The results presented in the following lead us to the conclusion that the response is dominated by resonant terahertz absorption at the plasma frequency sensed by a hot electron bolometer at the barrier.

5. Terahertz response

The resonant plasmonic response of the detector has been characterized using the broadly tunable, pulsed, narrow band UCSB free electron lasers (FEL). Unlike previous measurements, we have fixed the grating gate bias by shorting it to the source and have swept the THz frequency. For this work we used 2 μs pulse widths and tuned the FEL to fixed frequencies between 300 and 500 GHz in ∼10 GHz steps. The time-resolved response of the detector was measured with an oscilloscope as a change in source–drain voltage, δV_{SD}, under constant current bias. The signal was led from the detector and cryostat via coax, separated from the leads that delivered the DC constant current bias. Incident power or energy was measured using a THz frequency-independent Thomas–Keating energy detector. Response amplitude and time constant were extracted as a function of THz frequency and electrical bias.

Figure 3 shows the detector responsivity as a function of frequency. Here we explore the fundamental plasmon mode by sweeping frequency rather than sweeping grating gate voltage [9]. As reported by Shaner, the response depends in a qualitative and quantitative way on the direction of current flow. For $I_{SD} = -10\ \mu$A, the response is dominated by a pair of resonant features centered at 405 GHz with approximate total width of 40 GHz wide. There is a relatively weak but sharp feature on the high frequency shoulder and a broader feature at 395 GHz. When the bias current is reversed, $I_{SD} = +5\ \mu$A, the 395 GHz feature essentially disappears but the resonance at 420 GHz persists.

The sensitivity of the resonance at 395 GHz reproduces the observations of Shaner *et al* [9]; it appears only for electron flow from the grating gated region. With positive source drain bias, electrons travel away from the barrier and heating of the 2DEG by resonant excitation of 2D plasmons

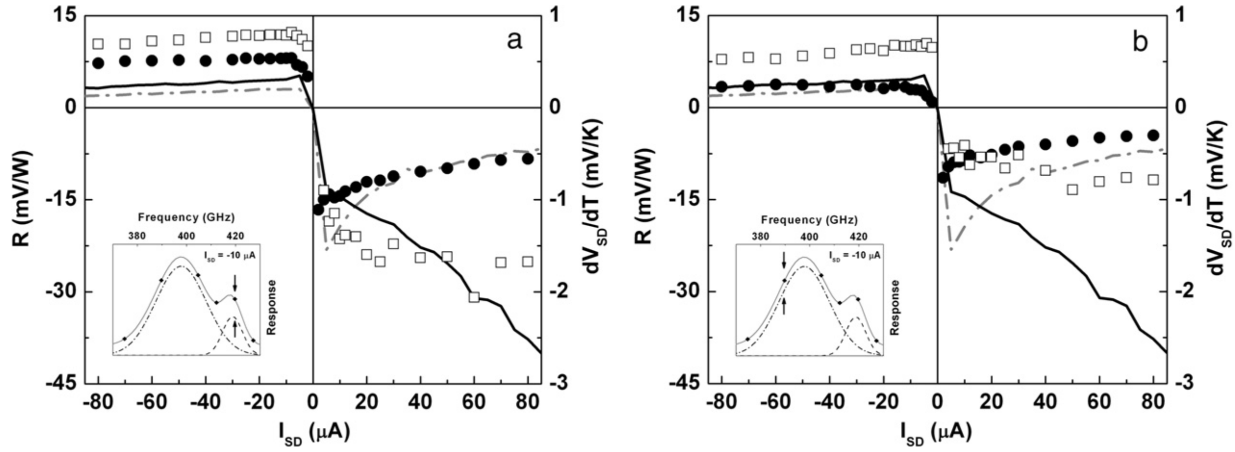

Figure 4. (a) 420 GHz detector response at 20 K with $V_{BG} = -650$ mV (circles) and $V_{BG} = -850$ mV (squares). (b) 390 GHz detector response at 20 K with $V_{BG} = -650$ mV (circles) and $V_{BG} = -850$ mV (squares). Device dV_{SD}/dT is also shown; the dashed gray line is for $V_{BG} = -650$ mV and the solid black line is for $V_{BG} = -850$ mV. Inset: arrows highlight the resonant feature we are characterizing under negative source–drain bias.

under the grating gate may not effectively thermally activate transport in the barrier region. We associate the 40 GHz wide resonance centered at 395 GHz with the grating gate voltage tuned resonances reported in previous work [5]. The full width at half-maximum is nearly an order of magnitude larger than that estimated from the mobility scattering rate [14]; radiation damping may account for this difference [12, 14].

The strength of the 420 GHz feature depends on bias direction but does not disappear for positive current flow. For positive source–drain bias it is 3–4 larger than the same feature with negative source–drain bias.

We also note that there is appreciable non-resonant response for positive bias. While the body of work reported on grating gated detectors leaves little doubt that the response is caused by resonant excitation of 2D plasmons, it is clear that our understanding of the absorption and detection mechanism is not complete.

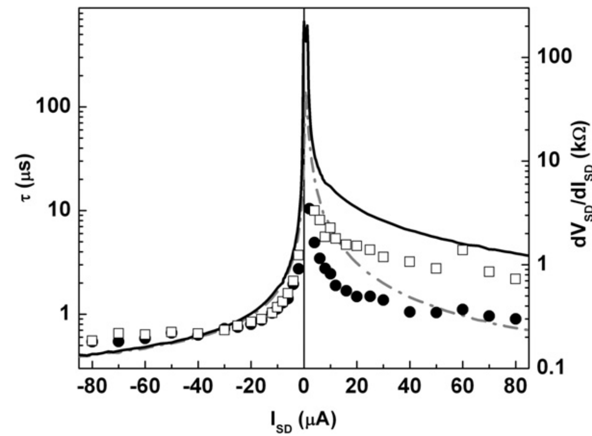

Figure 5. Detector time constant at 20 K with $V_{BG} = -650$ mV (circles) and $V_{BG} = -850$ mV (squares). Device differential resistance is also shown; the dashed gray line is for $V_{BG} = -650$ mV and the solid black line is for $V_{BG} = -850$ mV.

6. Results and discussion

To understand the detection mechanism in the pinched region of the channel, we explore response versus bias versus barrier gate voltage at 420 and 390 GHz and compare with a hot electron bolometer model. In figure 4(a) we display response measured with $V_{BG} = -650$ mV and $V_{BG} = -850$ mV at 20 K for 420 GHz radiation. In figure 4(b) we display response measured with $V_{BG} = -650$ mV and $V_{BG} = -850$ mV at 20 K for 390 GHz radiation. This data does not distinguish that the nature of the terahertz frequency response (resonant or non-resonant) depends on the direction of the current flow. In particular, the response at 390 GHz is plasmon resonant for negative currents but is best described as non-resonant background for positive current. The sharp resonant response at 420 GHz persists for either direction of current flow but appears in addition to the frequency-independent background for positive current flow.

Figure 5 displays the response time measured at 420 GHz for barrier gate voltages of −650 and −850 mV. The 420 and 390 GHz time constants at a given temperature, barrier gate voltage and bias current are indistinguishable; thus only the response times measured at 420 GHz have been shown. The response time spans nearly two decades from less than 1 μs to greater than 10 μs. Since the THz pulse width can be shorter or longer than the response time, depending on the bias point, we chose to correct the measured response as follows:

$$R = \frac{\delta V_{SD}}{P_{THz}} \left[1 - \exp\left(-t_{THz}/\tau\right)\right]^{-1} \tag{3}$$

where P_{THz} and t_{THz} are the THz pulse power and pulse width, respectively, and τ is the detector response time. Corrected in this way, the response in figure 4 is displayed as the signal that would have been detected had the THz pulse been on for a period long compared to the detector response time, $t_{THz} \gg \tau$.

To test the hot electron bolometer hypothesis, we compare the measured response defined in (3) to the rate of change of source–drain voltage with electron temperature. This model

assumes that the signal at fixed bias current is given by

$$\delta V_{SD} = \frac{\partial V_{SD}}{\partial T}\delta T \qquad (4)$$

where δT is the change in electron temperature induced by the absorbed radiation.

By measuring the I–V characteristics shown in figure 2 as a function of temperature around 20 K, $\frac{\partial V_{SD}}{\partial T}$ can be determined at different values of source–drain current. In figure 4 we show both the measured responsivity corrected as described in equation (3) and the measured $\frac{\partial V_{SD}}{\partial T}$. The sign of the response and qualitative behavior over a wide range of bias currents and different barrier gate voltages strongly suggest that the change in source–drain voltage across the pinched-off channel senses the change in electron temperature. Terahertz radiation is absorbed, the electron gas is heated and the temperature change causes a change in source–drain voltage. Because the nature of the terahertz absorption changes in a qualitative way with both frequency and current direction, it is not prudent to insist upon strong quantitative agreement.

It is tempting to also introduce terahertz rectification at the barrier and there may be some contribution from this mechanism. But we are not compelled to do so at this time.

The response time scales with the detector differential resistance, $\frac{\partial V_{SD}}{\partial I_{SD}}$, and can be closely but not perfectly described by a simple '*RC*', $\tau = C\frac{\partial V_{SD}}{\partial I_{SD}}$. This is well satisfied for all bias points and for different barrier gate voltages: $V_{BG} = -650$ mV and $V_{BG} = -850$ mV (figure 5). The capacitance is of the order of ~1 nF. We have not analyzed this capacitive load in detail, but the capacitance is comparable to estimates of the combined cable capacitance and the grating gate to channel capacitance.

The detector response time documented here is controlled by a combination of detector impedance and circuit capacitance, and we conclude that the intrinsic response time of the barrier and plasmonic absorber is faster than the fastest response time τ at any bias point. The intrinsic response time should be much less than 1 μs. On the other hand, if the entire detector, substrate and conduction electrons in the channel were being heated during the detection process, response times would be much longer and of the order of milliseconds. For the monolithic plasmonic absorber and planar barrier sensor terahertz detector discussed here, the bolometric response appears to be 'electrons only', a hot electron bolometer. The strong enhancement observed by Shaner *et al* [10] with membrane isolation for relatively much longer THz stimuli may represent heating of the lattice as well. This issue needs clarification.

A recent model of split-gate plasmonic detectors has been developed by Ryzhii *et al* [18] and features both bolometric and dynamic or rectified response. Without making a detailed comparison here, they conclude that both mechanisms are important but emphasize that temperature is the controlling parameter; elevated operating temperature favors rectification while low operating temperatures favor a bolometric response. The results presented here are not inconsistent with this model. Electron heating appears to play a definitive role in the response at low temperatures, although rectification may also be present at bias points where the device is highly nonlinear. Measurements of the response at elevated temperatures will be useful here. Operation at elevated temperatures will also determine if the detector can be used at temperatures that require less 'technology overhead' in the form of refrigeration.

7. Conclusions

We have characterized the THz response of an integrated SQW HEMT plasmonic THz detector with a voltage-controlled lateral barrier to enhance sensitivity. Swept THz frequency measurements exhibit a narrow, 40 GHz wide, plasmonic resonance centered at 405 GHz with an additional sharp feature at 420 GHz. The voltage-controlled barrier is biased beyond pinch off and the 'short-channel' source–drain IV characteristics with negative bias are similar to a planar Schottky diode. Regardless of the bias point, at 20 K the detection mechanism appears to be resonant heating of the electron gas sensed by transport over the barrier. The time constant is controlled by the detector differential resistance and circuit capacitance. While our understanding is not complete, these results taken in concert with previous work indicate that the lateral barrier plasmonic detector behaves as a narrow band THz hot electron bolometer. Optimization for responsivity, noise, speed, operating temperature and plasmon tuning are indicated.

Acknowledgments

The authors would like to thank Dave Enyeart and Gerry Ramian at the UCSB Free Electron Laser facility for their assistance, maintenance and operation of the facility. This work is supported by the University of Buffalo NSF-NIRT THz Collaboratory: ECS0609146. Sandia is a multiprogram laboratory operated by Sandia Corporation, a Lockheed Martin Company, for the United States Department of Energy's National Nuclear Security Administration under contract DE-AC04-94AL85000. Theoretical work is supported by ARO grant no. W911NF-05-1-0031.

References

[1] Dyakonov M and Shur M S 1996 *IEEE Trans. Electron Devices* **43** 380
[2] Teppe F, Veksler D, Kachorovski V Y, Dmitriev P, Xie X, Zhang X C, Rumyantsev S, Knap W and Shur M S 2005 *Appl. Phys. Lett.* **87** 022102
[3] Peralta X G, Allen S J, Wanke M C, Harff N E, Simmons J A, Lilly M P, Reno J L, Burke P J and Eisenstein J P 2002 *Appl. Phys. Lett.* **81** 1627
[4] Popov V V, Polischuk O V, Teperik T V, Peralta X G, Allen S J, Horing N J M and Wanke M C 2003 *J. Appl. Phys.* **94** 3556
[5] Shaner E A, Lee M, Wanke M C, Grine A D, Reno J L and Allen S J 2005 *Appl. Phys. Lett.* **87** 193507
[6] Shaner E A, Grine A D, Reno J L, Wanke M C and Allen S J 2008 *Laser Focus World* **44** 131

[7] Allen S J, Tsui D C and Logan R A 1977 *Phys. Rev. Lett.* **38** 980
[8] Tsui D C, Gornik E and Logan R A 1980 *Solid State Commun.* **5** 875
[9] Shaner E A, Grine A D, Wanke M C, Lee M, Reno J L and Allen S J 2006 *IEEE Photon. Technol. Lett.* **18** 1925
[10] Shaner E A, Wanke M C, Grine A D, Lyo S K, Reno J L and Allen S J 2007 *Appl. Phys. Lett.* **90** 181127
[11] Ando T, Fowler A B and Stern F 1982 *Rev. Mod. Phys.* **54** 437
[12] Aizin G R, Popov V V and Polischuk O V 2006 *Appl. Phys. Lett.* **89** 143512
[13] Aizin G R, Fateev D V, Tsymbalov M and Popov V V 2007 *Appl. Phys. Lett.* **91** 163507
[14] Shaner E A, Wanke M C, Lee M, Reno J L, Allen S J and Peralta X G 2005 *Proc. SPIE* **5790** 116
[15] Adams J A, Thayne I G, Wilkinson D W, Beaumont S P, Johnson N P, Kean A H and Stanley C R 1993 *IEEE Trans. Electron Devices* **40** 1047
[16] Ryzhii V and Shur M S 2006 *Japan. J. Appl. Phys.* **45** L1118
[17] Baumgartner P, Brunner K, Abstreiter G, Böhm G, Tränkle G and Weimann G 1993 *Appl. Phys. Lett.* **64** 592
Baumgartner P, Engel C and Abstreiter G 1996 *Appl. Phys. Lett.* **69** 76
Baumgartner P, Engel C, Böhm G and Abstreiter G 1997 *Appl. Phys. Lett.* **70** 2876
[18] Ryzhii V, Satou A, Otsuji T and Shur M S 2008 *J. Appl. Phys.* **103** 014504